做科研，非一朝一夕

买器材，应速战速决

Newport数千种优质产品当日发货，
更多惊喜尽在PhotonSpeed™光速购！

mks | Newport™

Femtosecond laser trapping dynamics of two-photon absorbing hollow-core nanoparticles

Liping Gong (贡丽萍)[1], Xiaohe Zhang (张笑河)[1], Zhuqing Zhu (朱竹青)[2], Guanghao Rui (芮光浩)[1], Jun He (何 军)[3], Yiping Cui (崔一平)[1], and Bing Gu (顾 兵)[1,4,*]

[1]*Advanced Photonics Center, Southeast University, Nanjing 210096, China*
[2]*Key Laboratory of Optoelectronic Technology of Jiangsu Province, School of Physical Science and Technology, Nanjing Normal University, Nanjing 210023, China*
[3]*School of Physics and Electronics, Central South University, Changsha 410012, China*
[4]*Collaborative Innovation Center of Light Manipulations and Applications, Shandong Normal University, Jinan 250358, China*
**Corresponding author: gubing@seu.edu.cn*

Received May 18, 2020; accepted June 10, 2020; posted online July 10, 2020

We investigate femtosecond laser trapping dynamics of two-photon absorbing hollow-core nanoparticles with different volume fractions and two-photon absorption (TPA) coefficients. Numerical simulations show that the hollow-core particles with low and high-volume fractions can easily be trapped and bounced by the tightly focused Gaussian laser pulses, respectively. Further studies show that the hollow-core particles with and without TPA can be identified, because the TPA effect enhances the radiation force, and subsequently the longitudinal force destabilizes the trap by pushing the particle away from the focal point. The results may find direct applications in particle sorting and characterizing the TPA coefficient of single nanoparticles.

Keywords: laser trapping; multiphoton processes; ultrafast nonlinear optics.
doi: 10.3788/COL202018.081901.

Core–shell nanostructures have received extensive attention due to their versatile compositions, structures, and properties for many significant applications in optics[1], biology[2], and catalysts[3]. Hereinto, hollow-core particles with diverse shell compositions present a class of special materials that brings a series of new opportunities. For example, the hollow Si particles are regarded as good candidates for controlled drug release[4]. Hollow Mo-doped SnO_2 nanoparticles improve the specific capacity in Li-ion batteries[5]. The hollow semiconductor particles, such as CdS or CdS/polystyrene composites, have shown the special quantum-confined effects, different either from the CdS quantum dots or the bulk counterparts[6]. Up to now, researchers have reported various design methods for fabricating hollow-core particles, including hard and soft template strategies[7,8]. It is noteworthy that the size of these hollow-core particles varies from tens to hundreds of nanometers, and the radius of the inner cavity can be arbitrarily controlled[9].

With the development of nanoscience and nanotechnology, investigations have been focused on optical trapping of various shapes and material compositions of small particles, such as dielectric particles[10], metal nanoparticles[11], carbon particles[12], quantum dots[13], living cells[14], and core–shell particles[1,15]. Using high-repetition-rate femtosecond-pulsed lasers instead of the conventional continuous-wave laser as the trapping light source, researchers have demonstrated how to enhance the trapping efficiency of Rayleigh particles[16], to split the trapping potential in the process of capturing gold nanoparticles[11], to reversibly trap and release the DNA[17], and to directionally eject optically trapped nanoparticles[16,18]. Essentially, these interesting optical trapping phenomena are related to the photophysical parameters of the particle itself and the surrounding environment as well as the laser characteristics, including the nonlinear optical properties of the trapped particle[19–21], the ambient optical nonlinearity[22], the pulse temporal shape[23], the distribution of the focal field[24], and the separation time between laser pulses[25].

By exploiting the photomechanical effect of laser beams, optical trapping technology realizes the optical manipulation of small particles, such as trapping[10], pushing[26], pulling[22,26], moving[27], rotating[28], hovering[29], ejecting[16], sorting[30], conveying[31], and axial reciprocating motion[32]. Due to its advantages of noncontact and noninvasive manipulation of particles, the optical trapping technique has wide applications in the characterization of single particles (e.g., position, motion, and morphology)[33], assembly of nanoparticles[34], measurement of viscosity of liquids[35], nonlinear refractive index measurement[36], etc.

In this work, we report the theoretical investigation on the optical trapping dynamics of two-photon absorbing hollow-core nanoparticles using tightly focused Gaussian laser pulses. We numerically study the optical forces on the hollow-core particles with different volume fractions and TPA coefficients. We analyze the trapping dynamic behaviors of two-photon absorbing hollow-core nanoparticles and discuss the underlying mechanisms.

It is assumed that the structure of a core–shell nanoparticle with an inner radius of a and an outer radius of b is embedded in water. Moreover, the core–shell nanoparticle

is a homogeneous, isotropic, non-magnetic sphere, and the optical nonlinearity originating from the particle instantaneously responds to femtosecond laser pulses. Hence, the effective permittivities of the core, shell, and surrounding environment are $\varepsilon^c = \varepsilon_0^c + \chi_3^c|\vec{E}(\vec{r},t)|^2$, $\varepsilon^s = \varepsilon_0^s + \chi_3^s|\vec{E}(\vec{r},t)|^2$, and ε_0^h, respectively. Here, χ_3^c and χ_3^s are the third-order nonlinear optical susceptibility of the core and the shell, respectively, and $\vec{E}(\vec{r},t)$ is the time-dependent electronic field around the particle. According to the Claussius–Mossotti relation and taking into account the radiative reaction correction[37], we yield the particle-induced dipole moment as

$$\vec{p}(\vec{r},t) = \alpha(\vec{r},t)\vec{E}(\vec{r},t), \tag{1}$$

$$\alpha(\vec{r},t) = \frac{\alpha_0(\vec{r},t)}{1 - i\alpha_0(\vec{r},t)k^3/(6\pi\varepsilon_0)}, \tag{2}$$

$$\alpha_0(\vec{r},t) = 4\pi\varepsilon_0 b^3 \frac{(\varepsilon^c + 2\varepsilon^s)(\varepsilon^s - \varepsilon_0^h) + f(\varepsilon^c - \varepsilon^s)(\varepsilon_0^h + 2\varepsilon^s)}{(\varepsilon^c + 2\varepsilon^s)(\varepsilon^s + 2\varepsilon_0^h) + 2f(\varepsilon^c - \varepsilon^s)(\varepsilon^s - \varepsilon_0^h)}, \tag{3}$$

where $k = 2\pi/\lambda$, λ is the wavelength, ε_0 is the permittivity of free space, and $f = a^3/b^3$ is the volume fraction. Specially, when $f = 0$ (or $f = 1$), Eq. (3) degenerates into the case of a solid particle reported previously[21]. Interestingly, the sign of the polarizability $\alpha_0(\vec{r},t)$ expressed by Eq. (3) could be positive or negative, which directly relates to the geometrical parameters and effective permittivity of the core–shell particle.

According to the dipole approximation theory[38], similar to the previous works reported in Refs. [21,22], we derive the time-averaged optical force exerted on the core–shell particle ($b \ll \lambda$) as

$$\langle \vec{F} \rangle = \frac{1}{4}\mathrm{Re}(\gamma)\nabla|\vec{E}_0(\vec{r})|^2 + \frac{k}{\varepsilon_0 c}\mathrm{Im}(\gamma)\langle \vec{S} \rangle_{\mathrm{Orb}}, \tag{4}$$

where

$$\langle \vec{S} \rangle_{\mathrm{Orb}} = \langle \vec{S} \rangle + \frac{\varepsilon_0 c}{2k}\mathrm{Im}\{[\vec{E}_0^*(\vec{r})\cdot\nabla]\vec{E}_0(\vec{r})\}, \tag{5}$$

$$\langle \vec{S} \rangle = \frac{1}{2\mu_0\omega}\mathrm{Im}\{\vec{E}_0(\vec{r}) \times [\nabla \times \vec{E}_0^*(\vec{r})]\}, \tag{6}$$

$$\gamma = \int_{-T/2}^{T/2} \alpha(\vec{r},t)\exp(-t^2/\tau^2)\mathrm{d}t. \tag{7}$$

Here, $\vec{E}_0(\vec{r})$ is the complex function of position in space, $\vec{E}_0^*(\vec{r})$ is the complex conjugate of $\vec{E}_0(\vec{r})$, c is the speed of light in vacuum, μ_0 is the permeability of free space, ω is the circular frequency, T is the pulse period (i.e., the inverse of the repetition-rate ν), and τ is the half-width at e^{-1} of the maximum for a Gaussian pulse.

As described by Eq. (4), optical forces on a core–shell particle with femtosecond laser pulses arise from two contributions: the gradient force and the radiation force. The gradient force, which is proportional to the gradient of optical intensity, drives the particle toward the equilibrium position. On the contrary, the radiation force, which is proportional to the orbital part of the Poynting vector of the field, destabilizes the trap. Note that, for the case of $f = 0$ (or $f = 1$), Eq. (4) degenerates into the ones reported previously for a solid particle without (or with) optical nonlinearity[21,39].

To trap and manipulate core–shell nanoparticles, we consider that an x-polarized Gaussian beam is tightly focused by a high numerical-aperture (NA) objective lens. Mathematically, one gets the three-dimensional electric field $\vec{E}_0(\vec{r})$ in the focal region of an aplanatic lens using the vectorial Debye theory[40]. In this case, one determines $\langle \vec{S} \rangle_{\mathrm{Orb}} = \langle \vec{S} \rangle$ along the propagation direction of the linearly polarized beam[21]. Consequently, the radiation force expressed by Eq. (4) is only proportional to the Poynting vector $\langle \vec{S} \rangle$. From Eq. (4), it is found that the gradient and radiation forces are proportional to the real and imaginary parts of the complex polarizability, $\mathrm{Re}(\gamma)$ and $\mathrm{Im}(\gamma)$, respectively. By adjusting the volume fraction f, in principle, one could determine the core–shell particle with an effective refractive index higher or lower than that of the ambience, resulting in the positive gradient force [i.e., $\mathrm{Re}(\gamma) > 0$] or the negative gradient force [i.e., $\mathrm{Re}(\gamma) < 0$]. Analogously, the radiation force depends on the volume fraction and the absorption losses due to both linear and nonlinear absorptions of the core–shell particles, leading to the positive radiation force [i.e., $\mathrm{Im}(\gamma) > 0$]. Consequently, it is expected to easily realize the trapping or pushing of a particle by manipulating both the volume fraction and TPA of the core–shell particle, as we will demonstrate below.

First, we consider an example of the CdTe/ZnTe core–shell particle immersed in water[41]. The linear permittivities of the core, shell, and surrounding medium are taken to be $\varepsilon_0^c = 8.64$ (for CdTe), $\varepsilon_0^s = 8.12$ (for ZnTe), and $\varepsilon_0^h = 1.77$ (for water), respectively. The third-order nonlinear refractive indexes and TPA coefficients of the core and shell are taken to be $n_2^c = -3 \times 10^{-17}$ m^2/W, $\alpha_2^c = 2.6 \times 10^{-10}$ m/W, $n_2^s = 1.2 \times 10^{-17}$ m/W, and $\alpha_2^s = 4.2 \times 10^{-11}$ m^2/W, respectively[42]. In this case, the real and imaginary parts of the third-order nonlinear optical susceptibility are related to the third-order nonlinear refractive index $n_2^{c/s}$ and TPA coefficient $\alpha_2^{c/s}$ through the conversion formulae $\mathrm{Re}[\chi_3^{c/s}] = 2n_2^{c/s}\varepsilon_0^{c/s}\varepsilon_0 c$ and $\mathrm{Im}[\chi_3^{c/s}] = \alpha_2^{c/s}\varepsilon_0^{c/s}\varepsilon_0 c/k$[43]. Without loss of generality, we take the following parameters unless otherwise mentioned as NA = 0.85, $b = 40$ nm, $\lambda = 800$ nm, $\tau = 100$ fs, $\nu = 76$ MHz, and the average power of laser pulses $P = 100$ mW for numerical simulations. Figure 1 gives examples of the optical force distributions on the core–shell particle for both the core and shell with and/or without optical nonlinearities when $f = 0.125$. It is shown that the distributions of the transverse and longitudinal optical forces originating from the optical nonlinearities of the core and/or shell are different from those of the core–shell particle in absence of the optical nonlinearity. The results can be understood as the following. Nonlinear refraction and nonlinear

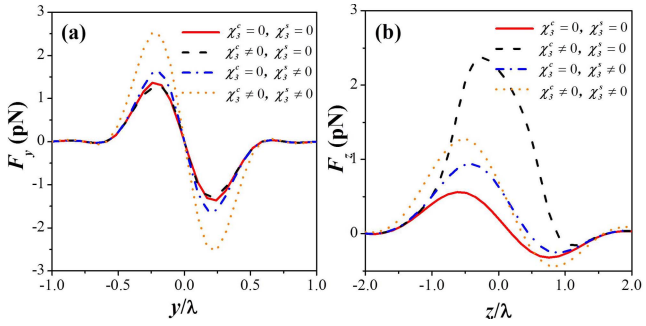

Fig. 1. (a) Transverse force profiles on the y axis ($x = z = 0$) and (b) longitudinal force profiles on the z axis ($x = y = 0$) for both the core and shell with and/or without optical nonlinearities when $f = 0.125$.

absorption are directly related to the real and imagery parts of the complex polarizability [i.e., Re(γ) and Im(γ)] and hence contribute to the gradient and radiation forces, respectively[22]. At the focal region, the transverse force mainly originates from the gradient force, whereas the longitudinal force arises from both the gradient and radiation forces[22].

As shown in Fig. 1, the optical force exerted on the core–shell particle with optical nonlinearity is rich, because this force strongly depends on the nonlinear refraction and nonlinear absorption of the core and shell, as well as the volume fraction. For the sake of simplicity, we focus our attention to a hollow-core nanoparticle immersed in water and investigate the optical forces on the particle by tightly focused x-polarized Gaussian beam. It is considered that the core is air, and the shell exhibits the third-order nonlinear refraction and TPA simultaneously. The typical values of the nonlinear refractive index and TPA coefficient in semiconductor nanoparticles are $n_2^s \sim 10^{-18}$ m^2/W and $\alpha_2^s \sim 10^{-11}$ m/W, respectively[44]. It is noted that the third-order nonlinear optical effects of both water and air are negligible and can be safely omitted in the analysis.

Under the assumption of the core without optical nonlinearity (i.e., $\chi_3^s = 0$) for the moment, we calculate the optical forces on the hollow-core nanoparticle with different volume fractions using Eq. (4). The trapping stiffness of the trapped particle at the equilibrium position, which is the quantity of interest for experimentalists, can be estimated by the Hook's law of $\kappa_j = F_j/r_j$, where r_j ($j = x, y, z$) is the distance from the equilibrium position. It is emphasized that the necessary criterion for stably trapping particles is the condition of $\kappa_j > 0$. Figure 2 shows the force distributions and trapping stiffness produced by tightly focused laser pulses for the hollow-core particle in absence of optical nonlinearity ($\chi_3^s = 0$) with different volume fractions f. Here, the transverse forces $\pm F_y$ (or longitudinal forces $\pm F_z$) in Figs. 2(a)–2(d) denote that their direction is along the $\pm y$ (or $\pm z$) direction. Interestingly, by tuning the volume fraction f from 0 to 1, the optical forces exerted on the hollow-core particle exhibit completely different characteristics. At small value

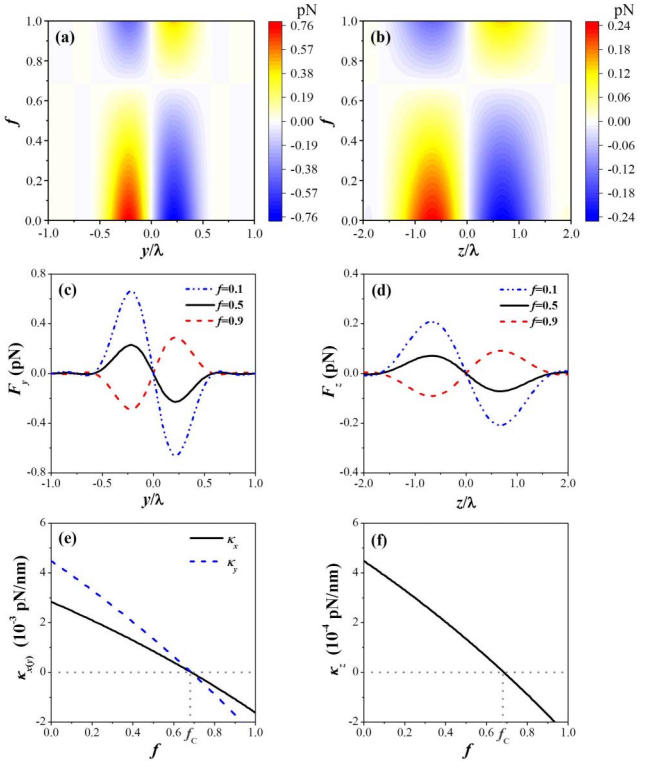

Fig. 2. Forces and trapping stiffness of the hollow-core particle in absence of optical nonlinearity ($\chi_3^s = 0$) with different volume fractions f. (a) Transverse force distributions on the y axis ($x = z = 0$) and (b) longitudinal force distributions on the z axis ($x = y = 0$) with different values of f. (c) Transverse force profiles on the y axis and (d) longitudinal force profiles on the z axis at three typical values of f. (e) Transverse and (f) longitudinal trapping stiffnesses as functions of f. The gray dotted lines in (e) and (f) are a guide for the eyes.

of f below a critical value f_c [see Figs. 2(e) and 2(f)], the hollow-core particle can be stably trapped by the tightly focused laser pulses at the focal point due to the existence of the equilibrium point in three-dimensional space. When the volume fraction exceeds f_c, however, this hollow-core particle could not be trapped by the focused Gaussian beam. The trapping behaviors of hollow-core particles can be understood as follows. The equivalent permittivity of a hollow-core particle $\varepsilon_0^{\rm eq}$ directly depends on the volume fraction f. For $f < f_c$ (or $f > f_c$), the hollow-core particle can be regarded as a high-refractive-index (or low-refractive-index) particle because of $\varepsilon_0^{\rm eq} > \varepsilon_0^h$ (or $\varepsilon_0^{\rm eq} < \varepsilon_0^h$). The conventional focused Gaussian beam is easy to realize the optical trapping of high-refractive-index particles[10], whereas it is not suitable to trap low-refractive-index particles[45]. Consequently, the hollow-core particles with low and high-volume fractions can easily realize the particle sorting. Figures 2(e) and 2(f) illustrate the transverse and longitudinal trapping stiffnesses as functions of f, respectively. For the trapped particle ($f < f_c$ and $\kappa_{x(y)} > 0$), κ_y is obviously larger than κ_x. This is due to the fact of $\kappa_j \propto |\vec{F}_j| \propto \nabla|\vec{E}_j|^2$. For the x-polarized Gaussian beam, the intensity gradient along the y axis $\nabla|\vec{E}_y|^2$ is a little

larger than $\nabla|\vec{E}_x|^2$ in the x axis[22]. Besides, as shown in Figs. 2(e) and 2(f), the smaller the volume fraction, the greater the trapping stiffness, and the more stable the trapped hollow-core particles. This is because the smaller the volume fraction, the closer the hollow-core particle is to the solid particle, and the larger the gradient force.

Now, we investigate the influence of the shell's optical nonlinearity on the trapping behavior of hollow-core particles. Figure 3 illustrates the optical forces and trapping potential produced by tightly focused laser pulses for a two-photon absorbing hollow-core particle immersed in water, taking the parameters of $f = 0.216$ (i.e., $a/b = 0.6$), $n_2^s = 1.2 \times 10^{-17}$ m^2/W, and different values of α_2^s. Regardless of the TPA effect, as shown in Figs. 3(a) and 3(c), the particles can be stably captured in the transverse plane, suggesting that the distributions of the transverse force are independent of α_2^s. The underlying mechanism can be understood as follows. The gradient force is mainly determined by the linear and nonlinear refractive indexes of both the particle and surrounding medium, while the radiation force depends on the linear and nonlinear absorption losses of the particle. The transverse force only originates from the gradient force, whereas both the gradient and radiation forces simultaneously contribute to the longitudinal force[22]. As the TPA effect becomes strong (i.e., the value of α_2^s increases), the radiation force gradually increases. Accordingly, as shown in Figs. 3(b) and 3(d), the longitudinal force exerted on a transversely confined particle experiences three stages: (i) for insignificant TPA, the particle is stably trapped at the focus; (ii) at relatively weak TPA process [see the solid line in Fig. 3(d)], the radiation force makes the equilibrium position of the particle deviate from the focus along the beam propagation direction; and (iii) with a strong TPA effect, the longitudinal force destabilizes the trap by pushing the particle in the direction of the beam's propagation. In order to quantitatively appraise the longitudinal dynamic behavior of the hollow-core particle, a longitudinal potential depth is estimated by $U_z = -\int F_z \mathrm{d}z$[21]. For the longitudinal trapping potential shown in Fig. 3(f), two important parameters are introduced, i.e., the absolute depth of the potential minimum $U_{\min}$ and the potential barrier U_{esc} that directly relates to the trapping efficiency. With the increasing of α_2^s, as shown in Fig. 3(e), the absolute depth of the potential minimum $U_{\min}$ becomes larger. However, the potential barrier U_{esc} also becomes shallower, resulting in the destabilization of the particle in the $+z$ direction. In a word, the hollow-core particles with and without TPA can be separated, because the TPA effect enhances the radiation force, and subsequently the longitudinal force destabilizes the trap by pushing the particle away from the focal point.

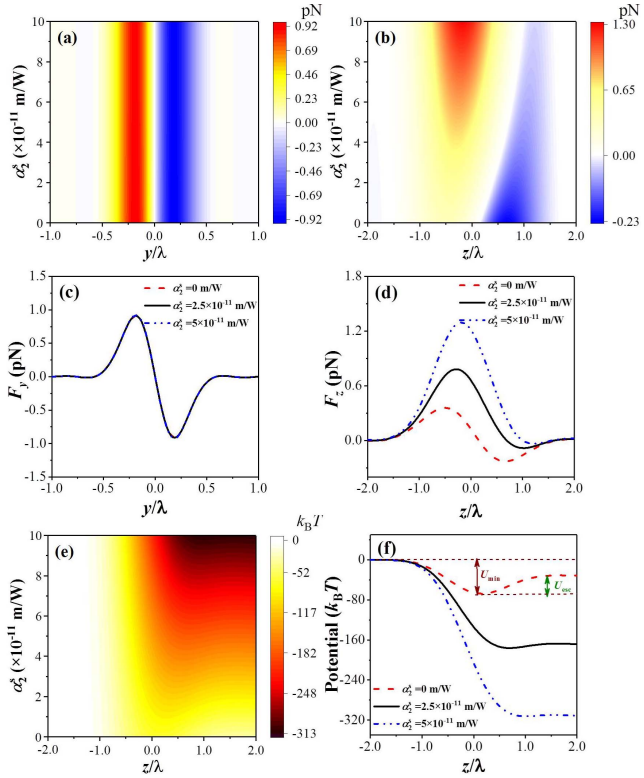

Fig. 3. Forces and longitudinal trapping potential of two-photon absorbing hollow-core particles at different TPA coefficients. (a) Transverse force distributions on the y axis ($x = z = 0$) and (b) longitudinal force distributions on the z axis ($x = y = 0$) with different values of α_2^s. (c) Transverse force profiles on the y axis and (d) longitudinal force profiles on the z axis at different values of α_2^s. (e) Distribution of longitudinal trapping potential on the z axis as a function of α_2^s. (f) Profiles of longitudinal trapping potential on the z axis at different values of α_2^s. The parameters for calculations are $f = 0.216$ and $n_2^s = 1.2 \times 10^{-17}$ m^2/W.

To observe the trapping dynamics of two-photon absorbing hollow-core nanoparticles, one could perform the optical trapping experiments at different powers of femtosecond laser pulses. Figure 4(a) illustrates the longitudinal force at the focal point $F_z(r = 0)$ as a function of laser power P and TPA coefficient α_2^s. At the focal point, the longitudinal force only arises from the radiation force. For a two-photon absorbing hollow-core particle, the radiation force mainly originates from the TPA effect.

The TPA effect enhances as the power increases. Subsequently, as shown in Fig. 4(b), the magnitude of $F_z(r = 0)$ is a nearly linear increasing function of P. Furthermore, the slope of this straight line directly relates to the TPA coefficient α_2^s. In the focal region of tightly focused femtosecond laser pulses, the longitudinal force enhanced by TPA destabilizes the trap by pushing the particles away from the focal point. With the known $F_z(r = 0)$, the velocity of the pushed particle v can be estimated from the force balance equation, $F_z(r = 0) + F_{\mathrm{fr}} = 0$, where $F_{\mathrm{fr}} = -6\pi\eta b v$ is the friction force[46]. Here, η is the dynamic viscosity of water (about 0.001 N · s · m^{-2} at room temperature). Figure 4(c) shows the velocity of a transversely confined particle at the focal point $v(r = 0)$ as a function of P and α_2^s. Similar to Fig. 4(b), by plotting $v(r = 0)$ as a function of P shown in Fig. 4(d), the slope of the straight line directly relates to the TPA coefficient α_2^s. The result suggests that one could pick up the TPA coefficient of a

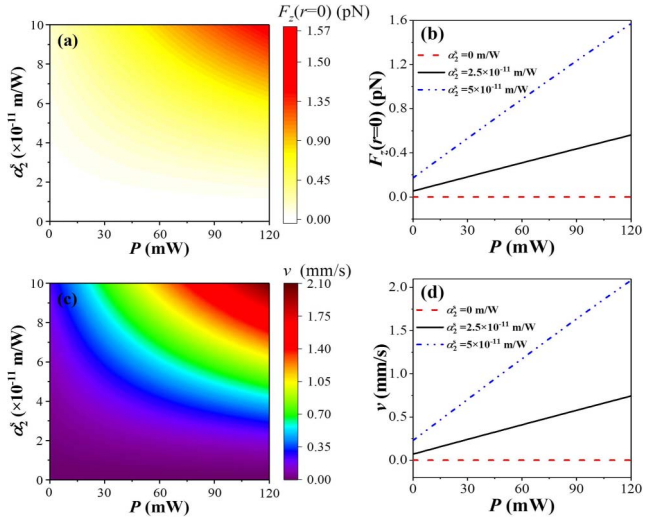

Fig. 4. Power-dependent longitudinal forces and velocities at the focal point for two-photon absorbing hollow-core particles with different TPA coefficients. (a) $F_z(r=0)$ against P and α_2^s. (b) Examples of power-dependent $F_z(r=0)$. (c) $v(r=0)$ against P and α_2^s. (d) Examples of power-dependent $v(r=0)$. The parameters for calculations are $f=0.216$ and $n_2^s=1.2\times10^{-17}$ m^2/W.

two-photon absorbing hollow-core nanoparticle from the measured $v(r=0)$ by performing the trapping dynamic experiments, although the treatment of such an inverse problem is relatively difficult. Nevertheless, the presented work may find direct application for characterizing the optical nonlinearity of single nanoparticles.

In summary, we investigated the optical forces produced by tightly focused laser pulses for the two-photon absorbing hollow-core nanoparticles with different volume fractions and TPA coefficients. It is shown that the hollow-core particles with low and high-volume fractions can easily be trapped and bounced by the tightly focused Gaussian laser pulses, respectively. We found that the TPA effect enhances the radiation force, and subsequently the longitudinal force destabilizes the trap by pushing the particle away from the focal point. In experiments, the trapping dynamics of two-photon absorbing hollow-core nanoparticles can realize the particle sorting and the TPA coefficient characterization of a single nanoparticle. First, the hollow-core particles with different volume fractions can easily be separated by a continuous-wave laser, where the optical nonlinearity is absent. The trapped and bounced hollow-core particles have low and high-volume fractions, respectively. Second, the above-mentioned trapped hollow-core particles with and without TPA can be sorted in the femtosecond laser trapping. The particles with TPA will be bounced off. Lastly, by measuring the velocity of the bounced particles at the focal point, one could estimate the TPA coefficient of a two-photon absorbing hollow-core particle.

This work was financially supported by the National Natural Science Foundation of China (No. 11774055) and the Natural Science Foundation of Jiangsu Province (No. BK20171364).

References

1. X. Bian, D. Gao, and L. Gao, Opt. Express **25**, 24566 (2017).
2. L. Zhou, J. Yuan, and Y. Wei, J. Mater. Chem. A **21**, 2823 (2011).
3. X. F. Zhang, X. L. Dong, H. Huang, B. Lv, X. G. Zhu, J. P. Lei, S. Ma, W. Liu, and Z. D. Zhang, Mat. Sci. Eng. A **454**, 211 (2007).
4. J. F. Chen, H. M. Ding, J. Wang, and L. Shao, Biomaterials **25**, 723 (2004).
5. X. Wang, Z. Li, Z. Zhang, Q. Li, E. Guo, C. Wang, and L. Yin, Nanoscale **7**, 3604 (2015).
6. M. Shao, D. Wang, B. Hu, G. Yu, and Y. Qian, J. Cryst. Growth **249**, 549 (2003).
7. Y. Liu, P. Yang, W. Wang, H. Dong, and J. Lin, Cryst. Eng. Comm. **12**, 3717 (2010).
8. L. Shen, L. Yu, X. Yu, X. Zhang, and X. Lou, Angew. Chem. Int. Ed. **54**, 1868 (2015).
9. A. El-Toni, M. A. Habila, J. Labis, Z. A. ALOthman, M. Alhoshan, A. A. Elzatahry, and F. Zhang, Nanoscale **8**, 2510 (2016).
10. A. Ashkin, J. M. Dziedic, J. E. Bjorkholm, and S. Chu, Opt. Lett. **11**, 288 (1986).
11. Y. Jiang, T. Narushima, and H. Okamoto, Nat. Phys. **6**, 1005 (2010).
12. B. He, X. Cheng, Y. Zhan, Q. Zhang, H. Chen, Z. Ren, C. Niu, J. Yao, T. Jiao, and J. Bai, EPL **126**, 64002 (2019).
13. W. Y. Chiang, T. Okuhata, A. Usman, N. Tamai, and H. Masuhara, J. Phys. Chem. B **118**, 14010 (2014).
14. X. Zhang, S. Yang, and L. Yuan, Chin. Opt. Lett. **17**, 090603 (2019).
15. M. C. Zhong, L. Gong, D. Li, J. H. Zhou, Z. Q. Wang, and Y. M. Li, Appl. Phys. Lett. **105**, 181112 (2014).
16. W. Y. Chiang, A. Usman, and H. Masuhara, J. Phys. Chem. C **117**, 19182 (2013).
17. T. Shoji, J. Saitoh, N. Kitamura, F. Nagasawa, K. Murakoshi, H. Yamauchi, S. Ito, H. Miyasaka, H. Ishihara, and Y. Tsuboi, J. Am. Chem. Soc. **135**, 6643 (2013).
18. W. Y. Chiang, A. Usman, T. Sugiyama, J. Hofkens, and H. Masuhara, J. Phys. Chem. C **122**, 13233 (2018).
19. T. Kudo and H. Ishihara, Phys. Rev. Lett. **109**, 087402 (2012).
20. A. Devi and A. K. De, J. Opt. **19**, 065504 (2017).
21. L. Gong, B. Gu, G. Rui, Y. Cui, Z. Zhu, and Q. Zhan, Photon. Res. **6**, 138 (2018).
22. L. Gong, X. Zhang, B. Gu, Z. Zhu, G. Rui, J. He, Q. Zhan, and Y. Cui, Nanophotonics **8**, 1117 (2019).
23. J. C. Shane, M. Mazilu, W. M. Lee, and K. Dholakia, Opt. Express **18**, 7554 (2010).
24. L. Wang and H. Chai, Opt. Express **19**, 14389 (2011).
25. T. H. Liu, W. Y. Chiang, A. Usman, and H. Masuhara, J. Phys. Chem. C **120**, 2392 (2016).
26. J. Lu, H. Yang, L. Zhou, Y. Yang, S. Luo, Q. Li, and M. Qiu, Phys. Rev. Lett. **118**, 043601 (2017).
27. A. A. Kovalev, V. V. Kotlyar, and A. P. Porfirev, Opt. Lett. **41**, 2426 (2016).
28. Y. Zhang, Y. Xue, Z. Zhu, G. Rui, Y. Cui, and B. Gu, Opt. Express **26**, 4318 (2018).
29. B. He, X. Cheng, H. Zhang, H. Chen, Q. Zhang, Z. Ren, S. Ding, and J. Bai, Appl. Phys. Express **11**, 052501 (2018).
30. A. Devi and A. K. De, J. Opt. **21**, 065502 (2019).
31. B. Hadad, S. Froim, H. Nagar, T. Admon, Y. Eliezer, Y. Roichman, and A. Bahabad, Optica **5**, 551 (2018).
32. Z. Liu, T. Wang, Y. Zhang, X. Tang, P. Liu, Y. Zhang, X. Yang, J. Zhang, J. Yang, and L. Yuan, Chin. Opt. Lett. **16**, 053501 (2018).
33. Z. Gong, Y. L. Pan, G. Videen, and C. Wang, J. Quant. Spectrosc. **214**, 94 (2018).

34. Z. Yan, M. Sajjan, and N. F. Scherer, Phys. Rev. Lett. **114**, 143901 (2015).
35. A. Statsenko, W. Inami, and Y. Kawata, Opt. Commun. **402**, 9 (2017).
36. S. Birzhandi, K. Madanipour, and S. Ghanbari, Opt. Commun. **444**, 154 (2019).
37. B. T. Draine, Astrophys. J. **333**, 848 (1988).
38. P. Chaumet and M. Nieto-Vesperinas, Opt. Lett. **25**, 1065 (2000).
39. S. Albaladejo, M. I. Marqués, M. Laroche, and J. J. Sáenz, Phys. Rev. Lett. **102**, 113602 (2009).
40. M. Gu, *Advanced Optical Imaging Theory* (Springer, 2000), Chap. 6.
41. S. Rawalekar, S. Kaniyankandy, S. Verma, and H. N. Ghosh, J. Phys. Chem. C **115**, 12335 (2011).
42. A. A. Said, M. Sheik-Bahae, D. J. Hagan, T. H. Wei, J. Wang, J. Young, and E. W. Van Stryland, J. Opt. Soc. Am. B **9**, 405 (1992).
43. M. Sheik-Bahae, A. A. Said, T. H. Wei, D. J. Hagan, and E. W. Van Stryland, IEEE J. Quantum Elect. **26**, 760 (1990).
44. D. N. Christodoulides, I. C. Khoo, G. J. Salamo, G. I. Stegeman, and E. W. Van Stryland, Adv. Opt. Photon. **2**, 60 (2010).
45. G. Rui, Y. Wang, X. Wang, B. Gu, and Y. Cui, J. Phys. Commun. **2**, 065015 (2018).
46. G. Tkachenko, I. Toftul, C. Esporlas, A. Maimaiti, F. L. Kien, V. G. Truong, and S. N. Chormaic, Optica **7**, 59 (2020).